Catalysis Today 171 (2011) 116–125

Contents lists available at ScienceDirect

Catalysis Today

journal homepage: www.elsevier.com/locate/cattod

Low temperature steam reforming of methane over metal catalyst supported on $Ce_xZr_{1-x}O_2$ in an electric field

Yasushi Sekine*, Masayuki Haraguchi, Masahiko Matsukata, Eiichi Kikuchi

65-301A, 3-4-1, Okubo, Shinjuku, Tokyo 169-8555, Japan

ARTICLE INFO

Article history:
Received 31 October 2010
Received in revised form 18 February 2011
Accepted 29 March 2011
Available online 2 June 2011

Keywords:
Steam reforming of methane
Low temperature reaction
Electreforming
$Ce_xZr_{1-x}O_2$ oxide
Hydrogen production

ABSTRACT

Catalytic steam reforming of methane in an electric field (named "electreforming") was conducted over metal catalysts supported on CeO_2 or $Ce_xZr_{1-x}O_2$ at low temperatures such as 423 K where conventional catalytic reactions hardly proceeded. The conversion of methane was greatly increased by weak and effective application of an electric field to the catalyst bed. Use of $Ce_xZr_{1-x}O_2$ as a catalyst support promoted electreforming, the lattice oxygen of $Ce_xZr_{1-x}O_2$ playing an important role. Energy efficiency of electreforming, reaction mechanism, and the role of lattice oxygen were investigated and are discussed in this paper.

1. Introduction

Hydrogen production from various primary energy sources such as fossil fuels and biomass is very important technology to meet future energy demand. Today, the major process of hydrogen production is catalytic steam reforming of methane. The reaction is highly endothermic and requires high temperature. Normally, steam reforming of methane is conducted at very high temperature like as 973–1123 K with supported Ni catalyst [1–11]. High temperature processes require long start-up time for heating the catalyst bed, a heat-exchanger for achieving higher energy efficiency. Small commercial devices require quick start-up and simple processes, so use of high temperatures has serious problems. Therefore, a catalytic process that works at lower temperatures is desired, and it is also required that the process has high energy efficiency and fast-startup feature. Up to now, many processes have been proposed for low temperature hydrogen production as shown in Fig. 1. Processes for rapid start-up of the reaction by internal heat include oxidative reactions like as partial oxidation of methane/hydrocarbons to produce syngas (H_2 and CO), autothermal reforming, oxidative steam reforming (so called oxyreforming). Some researchers have investigated autothermal reforming [12–15] and partial oxidation [16–20] of methane/hydrocarbons to produce synthesis gas at lower temperatures of 773–973 K. These reactions can be conducted at lower temperatures than steam reforming of methane, but their use of exothermic reactions (oxidation) lowers the fuel's calorific value. On the other hand, EHC (electrically heated catalyst) process for cold start has been investigated in 1990s for the rapid heating of the catalyst bed by external heat to increase the catalytic activity [21–23]. Also, many investigations for the application of low-temperature non-equilibrium plasma [24–33], electrochemical catalytic reactions, especially non-Faradaic electrochemical modification of catalytic activity (NEMCA) [34–47], have been conducted to promote the catalytic reaction at low temperature. Plasma-aided catalytic reaction is very promising at low gas phase temperature, but it is hard to enlarge the reaction system due to the structure of the reactor and the electric power consumption. NEMCA process is also very attractive for its high activity, but it has been conducted at higher temperature to produce O^{2-} or Na^+, F^- or other mobile ions on the solid oxide surface. To solve such problems, we have investigated an application of an electric field to conduct catalytic steam reforming of methane/hydrocarbon/alcohol at low temperatures like as 423 K [48,49]. Because an electric field requires less energy than other methods of application of electricity such as plasma or electrolysis, the reaction can be conducted in milder conditions. To date, we have found that highly efficient and low-temperature catalytic degradation of ethanol in an electric field is achievable at lower temperatures of about 573 K [48]. The reaction proceeds in a lower temperature region in which conventional catalytic reactions cannot occur. Because products show a similar trend of conventional catalytic process, the reaction is easily controlled by the nature of catalyst [49]. Applying this novel reaction system to a conventional catalytic system, selective catalytic reaction can proceed

* Corresponding author. Tel.: +81 3 5286 3114; fax: +81 3 5286 3114.
E-mail address: ysekine@waseda.jp (Y. Sekine).

0920-5861/$ – see front matter © 2011 Elsevier B.V. All rights reserved.
doi:10.1016/j.cattod.2011.03.076

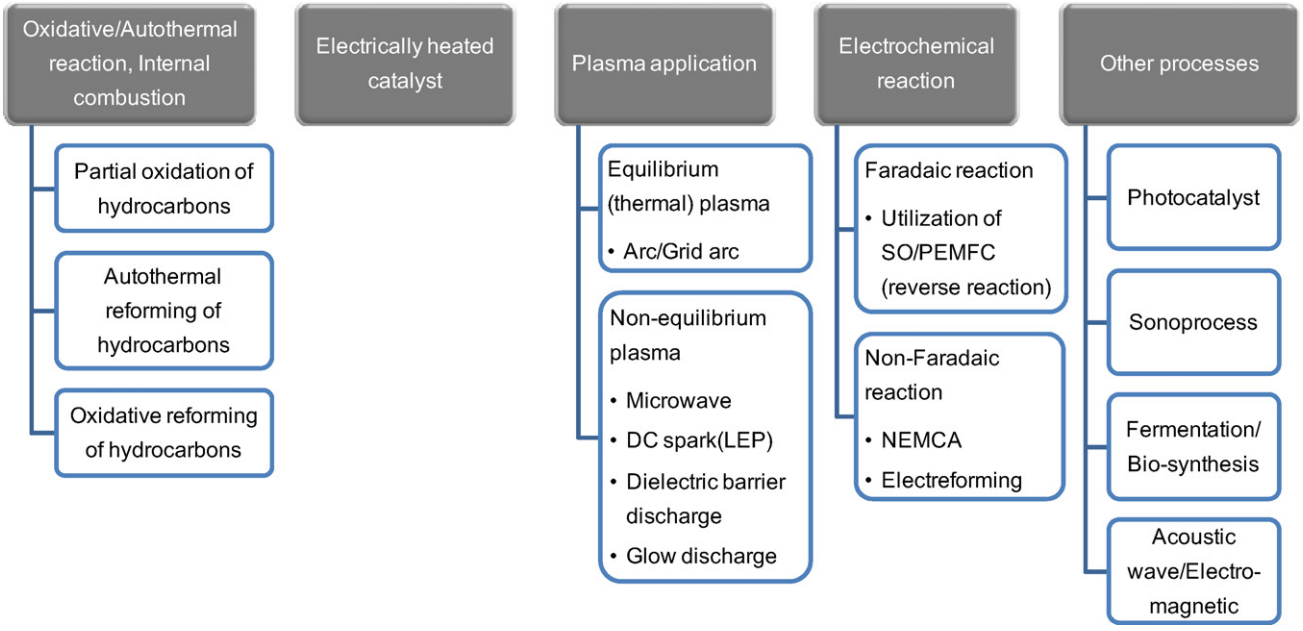

Fig. 1. Low temperature hydrogen production processes from hydrocarbons.

using low-temperature-wasted-heat which has not been used so far.

In this paper, a conventional catalytic reaction and a catalytic reaction in an electric field (electreforming) were performed and compared for the steam reforming of methane at low temperatures such as 423 K. Thermodynamic equilibrium remits the methane conversion at a very low level under such a low temperature. Steam reforming of methane is a highly endothermic reaction and requires high temperatures.

$$CH_4 + 2H_2O \rightarrow CO_2 + 4H_2 \quad \Delta H_{298} = 164.9\,\text{kJ mol}^{-1} \tag{1}$$

In previous studies, we have found that noble metals such as Pt show high catalytic performances for steam reforming of hydrocarbons in the electric field. Therefore, we chose Pt, Rh, Pd and Ni as supported metals and CeO_2, $Ce_xZr_{1-x}O_2$ and other oxides as a catalyst support based on its properties of dielectric constant and other catalytic characteristics.

2. Experimental

2.1. Catalyst preparation

All the catalysts used in this study were prepared by an impregnation method with an aqueous solution of metal precursor and an oxide support. For the catalyst support, we applied $Ce_xZr_{1-x}O_2$ (x = 1, 0.75, 0.5, 0.25, 0) prepared by co-precipitation method of $Ce(NO_3)_3{\cdot}6H_2O$ and $ZrO(NO_3)_2{\cdot}2H_2O$ with NH_3aq. After a precipitate was obtained, it was well-washed and calcined at 973 K for 3 h to form $Ce_xZr_{1-x}O_2$ oxide phase. Perovskite oxide $SrTiO_3$ was also used as a catalyst support, and it was prepared using a complex polymerization method as follows: the precursors (Kanto Kagaku Corp.) of perovskite-type oxides, $[(CH_3)_2CHO]_4Ti$, $Sr(NO_3)_2$, were dissolved in distilled water, then citric acid and ethylene glycol were added to the solution. The obtained solution was dried to produce a gel and was pre-calcined at 673 K, then calcined at 1123 K for 10 h.

For the impregnation of metal onto the support, an aqueous solution of metal precursor (for Pt, $Pt(NH_3)_4(NO_3)_2$, for Rh, $Rh(NO_3)_3$, for Ni, $Ni(NO_3)_2{\cdot}6H_2O$ was used) or an acetone solution of $Pd(OCOCH_3)_2$ was used to support 1 wt % of metal onto the support (only for Ni, 10 wt% of Ni was impregnated). The produced oxide powder was soaked in water for 2 h for deaeration before the impregnation of metal. A mixture of catalyst-support and liquid solution of the precursor was heated on the stirrer and evaporated to dryness. The resultant powder was dried in an oven at 393 K for 20 h in air. Then, it was calcined in a muffle furnace at 973 K for 12 h. Obtained powdery catalyst was pressed at 60 kg N for 10 min then it was crushed and sieved into particles of 355–500 μm.

2.2. Catalytic activity test with/without an electric field

All experiments for the catalytic activity test were conducted in a fixed bed flow-type reactor. A schematic image of the reaction system of electreforming is shown in Fig. 2. Two stainless steel rods were inserted from each end of the quartz tube as electrodes. A quartz tube of 8.0 mm o.d. was used as a reactor and SUS304 rods 2.0 mm o.d. were used as electrodes. Reaction flow was a mixture of $CH_4/H_2O/Ar$ = 12/24/18 SCCM, total space velocity (GHSV) was 22,500 h^{-1} and steam/carbon ratio (S/C) was 2. A 200 mg of the catalyst was charged in the reactor and fixed by quartz wool. The catalyst bed height was about 4 mm; the gap distance of each electrode was 5 mm. Consequently, the catalyst bed did not contact with the tip of the upper electrode. The catalyst was not pre-treated (reduced) before the electreforming reaction because we did not find any difference of activity between a pre-reduced catalyst and an as-calcined catalyst on the electreforming. Steam was supplied using a micro-feeder and evaporated in a pre-heating zone, carried with Ar. The product gases were analyzed using a gas chromatograph-FID and -TCD after passing a cold trap. In this study, methane conversion was calculated from products. No carbon deposition was observed in any reactions. A DC high voltage power supply was used to generate an electric field. The electric field was controlled by changing the input current, and 3 mA of current was applied to the catalyst bed in this work. Regarding the controlling parameter for the electreforming, the superimposed electric pressure depended on the nature of the catalyst. The total input power (=electrical power consumption) was calculated and shown independently in the results (Tables 2–6). Waveforms of the current and voltage were observed using a digital signal oscilloscope (TDS3052B; Tektronix Inc.). Each profile of the current and

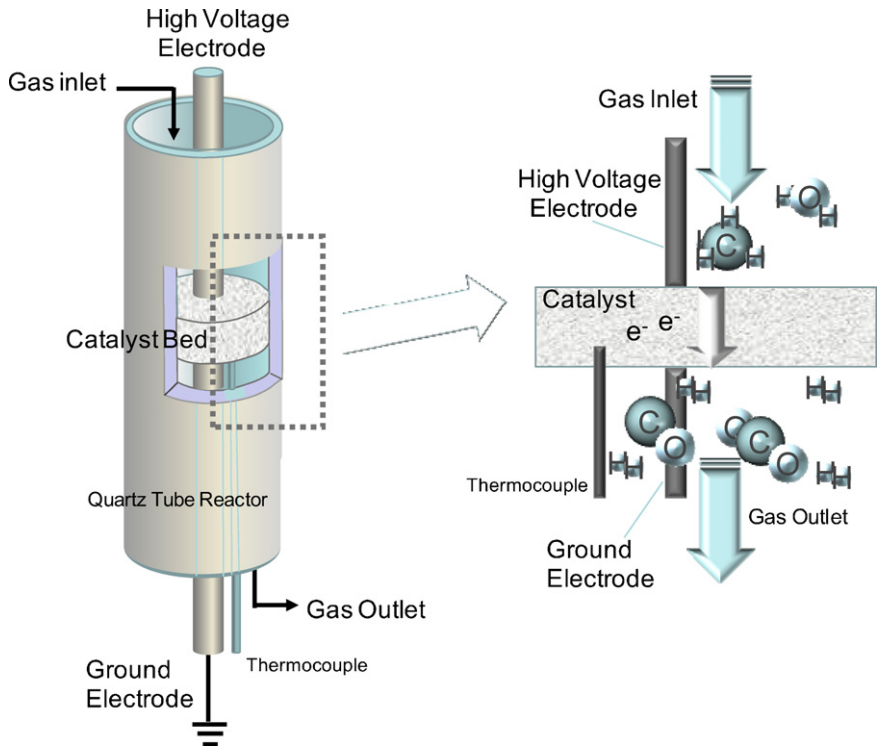

Fig. 2. Schematic image of the electreforming system.

voltage was flat and no plasma/discharge was observed under any conditions of electreforming.

Methane conversion and yield of product are calculated from the amount of products by following equation:

$$\text{yield of product}\,(\%) = \frac{\text{moles of produced amount of product}}{\text{input moles of methane}} \times 100 \quad (2)$$

$$\text{H}_2\ \text{yield}\,(\%) = \frac{\text{moles of produced hydrogen}}{\text{input moles of methane}} \times 100 \quad (3)$$

So, maximum hydrogen yield is 400% by regarding Eq. (1).

Enthalpy gain of the electreforming ΔE_{ef} was calculated by the following equation:

$$\Delta E_{ef} = \left[\left\{\sum \Delta H_p\,(\text{electreforming}) - \Delta H_{CH4}\ (\text{electreforming})\right\} - \left\{\sum \Delta H_p\,(\text{catalytic reaction}) - \Delta H_{CH4}\,(\text{catalytic reaction})\right\}\right] \quad (4)$$

following terms represent; $\sum \Delta H_{p\,(\text{electreforming})}$: summation of heating values of products on electreforming, $\Delta H_{CH4\,(\text{electreforming})}$: heating value of consumed methane on electreforming, $\sum \Delta H_{p\,(\text{catalytic reaction})}$: summation of heating values of products on catalytic reaction (i.e. almost zero at low temperature), $\Delta H_{CH4\,(\text{catalytic reaction})}$: heating value of consumed methane on catalytic reaction (i.e. almost zero at low methane conversion).

This ΔE_{ef} corresponds to the consumed energy which contributes to the endothermic reaction (steam reforming of methane; Eq. (1)).

2.3. Characterization of catalyst

Characterization of the prepared catalyst was conducted using following methods; for monitoring the structure of the catalyst and evaluating the particle diameter, X-ray diffractometer (XRD: Rint-2000; Rigaku Corp.) with CuKα radiation using 40 kV/20 mA current. Specific surface areas of catalysts were measured using N_2 adsorption at 77 K. The samples were outgassed at 573 K for 2 h prior to N_2 adsorption. Calculated specific surface areas are summarized in Table 1 and discussed in latter section. For measuring the reducibility of catalyst support, temperature programmed reduction (TPR) was conducted using a thermogravimetric analyzer (TG: TGA-50, SHIMADZU corp.) under the flow of 10%H_2/90%N_2 at 50 cc min^{-1}. Samples were pre-heated in situ at 323 K for 15 min to desorb the adsorbed water, then heated to 873 K at the heating rate of 10 K min^{-1}.

3. Results and discussion

3.1. Effect of an electric field for catalytic steam reforming over metal catalysts supported on CeO_2

First, the conventional catalytic steam reforming of methane with/without an electric field was performed at low temperatures from 423 K to 773 K. Because the equilibrium constant of endothermic steam reforming of methane was quite small in the low temperature range of 423–573 K, the thermodynamic equilibrium conversion of methane under these conditions is very small, for example only 0.5% at 423 K.

Fig. 3 shows the conversion of methane for each metal catalyst (Pt, Pd, Rh – 1 wt%, Ni – 10 wt%) supported on CeO_2 in the presence or absence of the electric field. In this figure, the open symbols represent results for the catalytic reactions without the electric field

Table 1
BET specific surface areas of $Ce_xZri_{1-x}O_2$ supports.

Catalyst support	Specific surface area ($m^2\ g^{-1}$)
CeO_2	7.2
$Ce_{0.75}Zr_{0.25}O_2$	42.9
$Ce_{0.5}Zr_{0.5}O_2$	53.2
$Ce_{0.25}Zr_{0.75}O_2$	55.0
$SrTiO_3$	18.8

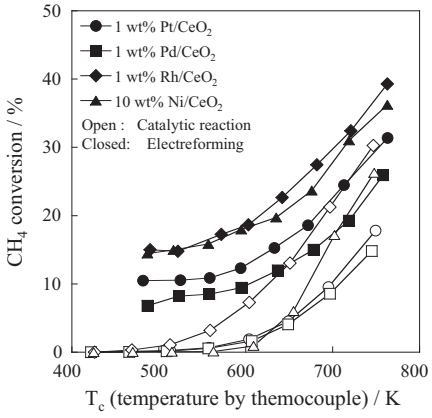

Fig. 3. Methane conversion versus temperature measured by a thermocouple for various metal catalysts supported on CeO_2 in the absence or presence of an electric field.

and closed symbols represent results with the electric field (=electreforming). Methane conversion for the catalytic reaction without the electric field was almost zero at such a low temperature like as 423 K. These four catalysts showed little or no activity at 423–573 K. By applying the electric field for the catalyst bed, steam reforming of methane proceeded and methane conversion increased drastically. The effect of the electric field was larger for the Rh/CeO_2 catalyst. The methane conversion for electreforming was 15.0% at 490 K over Rh/CeO_2, 14.5% at 487 K over Ni/CeO_2. The catalyst bed temperature was measured by a thermocouple. The maximum conversion in this range of the reaction temperature was 39.3% at 763 K over Rh/CeO_2 for the electreforming. These conversions for the electreforming exceeded the corresponding thermodynamic equilibrium conversion at each temperature. Fig. 4 shows the yield of products over each catalyst. In addition, a calculated yield based on the thermodynamic equilibrium at a certain temperature (shown in the figure) was indicated at the right-end in each figure. From Fig. 4, it can be seen that both catalytic reactions and the electreforming produced H_2, CO_2 and a little amount of CO. Product gas composition in both cases corresponded to about 80% of H_2, 20% of CO_2 and few percents of CO. The selectivity to these products was similar in the presence or absence of the electric field. Products were practically only H_2 and CO_2 at conversion lower than 20%, however, the ratio of CO to CO_2 increased for all catalysts with the increase of methane conversion.

Table 2 shows the formation rate of products and the endothermic enthalpy gain, ΔE_{ef}, which was calculated the difference of endothermic enthalpy between electreforming and catalytic reaction at each reaction temperature over Pt/CeO_2 or $Pt/SrTiO_3$ perovskite. These energies at 423–473 K were 10.1–10.5 J min^{-1} for the Pt/CeO_2 catalyst, 9.1–10.4 J min^{-1} for the Pd/CeO_2 catalyst, 18.8–19.7 J min^{-1} for the Rh/CeO_2 catalyst, and 16.9–17.9 J min^{-1} for the Ni/CeO_2 catalyst, respectively. The input electric energies at 423–473 K were 99.9–101.0 J min^{-1} (=1.66–1.68 W; Pt/CeO_2), 91.9–96.5 J min^{-1} (=1.53–1.61 W; Pd/CeO_2), 82.6–94.0 J min^{-1} (=1.38–1.57 W; Rh/CeO_2), and 92.1–99.4 J min^{-1} (=1.54–1.66 W; Ni/CeO_2). Therefore, the endothermic enthalpy gain by the electric field over metal catalysts supported on CeO_2 was about 10–20% of the input electric energy, and metal catalysts supported on $SrTiO_3$ perovskite showed lower energy efficiency than CeO_2 for the electreforming.

3.2. *Effect of Zr-doping into CeO_2 support*

Zr-doped ceria ($Ce_xZr_{1-x}O_2$) is known to be a good catalyst support due to its redox ability. So we investigated the effect of

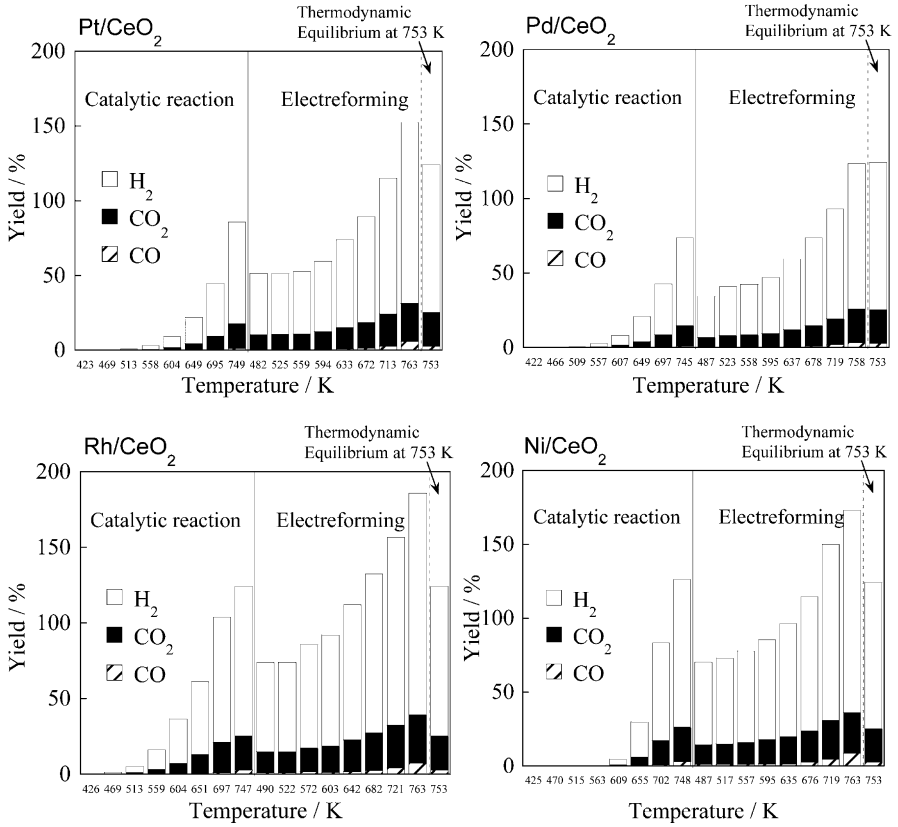

Fig. 4. Hydrogen, CO and CO_2 yield as a function of temperature measured by a thermocouple over various metal catalysts supported on CeO_2 in the absence or presence of an electric field.

Table 2
Activities and energy balances for various metal catalysts supported on CeO_2 or $SrTiO_3$ in the presence or absence of an electric field at 423 K of furnace temperature.

	EF[a]	T_{tc}[b] (K)	CH_4 conv. (%)	ΔH_{CH4} (J min^{-1})	EPC[c] (W)	Formation rate (μmol min^{-1})			H_2/(3CO + 4CO_2)	$\sum \Delta H^d_p$ (J min^{-1})	ΔH^e_r (J min^{-1})	ΔE_{ef} (J min^{-1})
						H_2	CO_2	CO				
Pt/CeO_2	No	423	0.0	0.0	–	0.0	0.0	0.0	–	0.0	0.0	
	With	482	10.5	47.6	1.66	200.3	48.3	3.0	1.0	58.1	10.5	10.5
Pd/CeO_2	No	422	0.0	0.0	–	0.0	0.0	0.0	–	0.0	0.0	
	With	487	6.8	29.4	1.61	134.1	32.2	0.8	1.0	38.6	9.1	9.1
Rh/CeO_2	No	426	0.0	0.0	–	0.0	0.0	0.0	–	0.0	0.0	
	With	490	15.0	67.3	1.38	296.2	70.5	5.1	1.0	86.1	18.8	18.8
Ni/CeO_2(10wt%)	No	425	0.0	0.0	–	0.0	0.0	0.0	–	0.0	0.0	
	With	487	14.5	65.0	1.66	281.4	67.9	5.1	1.0	81.9	16.9	16.9
$Pt/SrTiO_3$	No	415	0.0	0.0	–	0.0	0.0	0.0	–	0.0	0.0	
	With	457	4.9	20.8	1.97	95.9	19.1	4.3	1.1	28.6	7.9	7.9
$Pd/SrTiO_3$	No	414	0.0	0.0	–	0.0	0.0	0.0	–	0.0	0.0	
	With	466	13.1	54.7	1.93	225.0	30.1	31.4	1.0	73.2	18.4	18.4
$Rh/SrTiO_3$	No	425	0.0	0.0	–	0.0	0.0	0.0	–	0.0	0.0	
	With	496	22.4	102.9	2.32	431.8	88.4	23.2	1.0	133.0	30.0	30.0

[a] EF: electric field.
[b] T_{tc}: catalyst bed temperature measured by a thermocouple.
[c] EPC: electric power consumption for the electric field.
[d] $\sum \Delta H_p$: summation of the heating values of products.
[e] ΔH_r: difference of the heating rate of products and consumed methane.

Zr-doping into CeO_2 support on the electreforming. The catalytic activity of $Pt/Ce_xZr_{1-x}O_2$ with different zirconium content ($x = 0$, 0.25, 0.5, 0.75, 1) was examined in order to investigate the effect of Zr-doping. Fig. 5 shows the conversion of methane for the catalytic reaction without the electric field and for the electreforming over $Pt/Ce_xZr_{1-x}O_2$ catalyst. Although the activity of catalytic reaction without the electric field was not affected by the introduction of ZrO_2, the activity was drastically promoted by the introduction

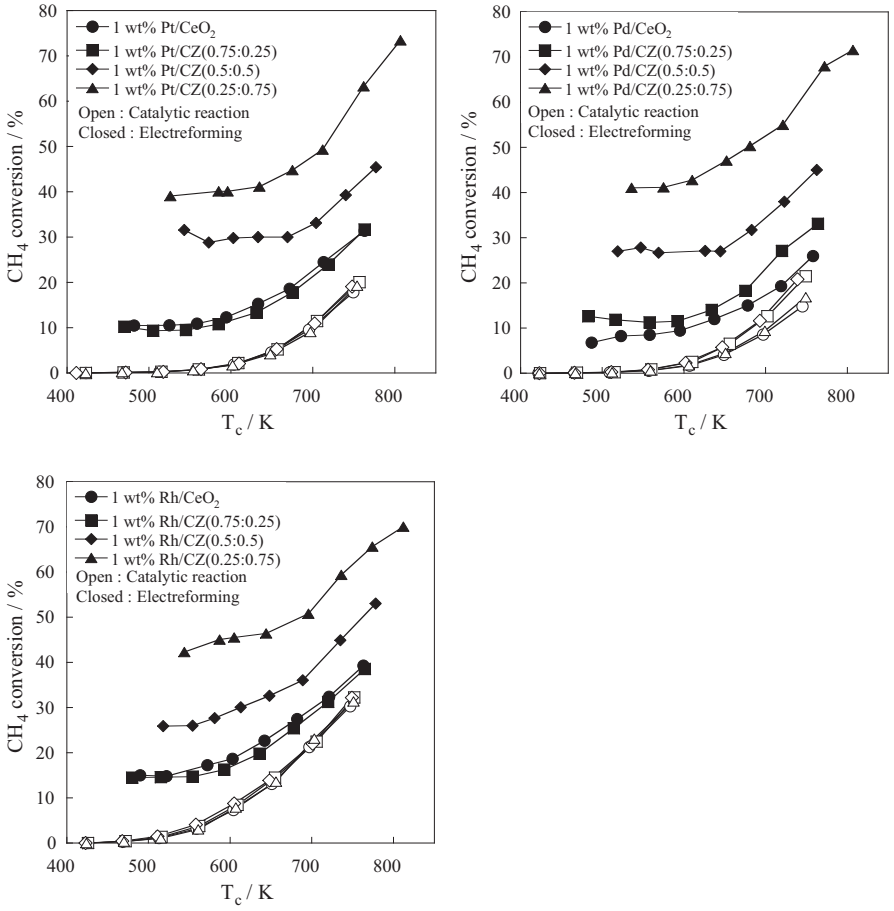

Fig. 5. Methane conversion versus temperature measured by a thermocouple for Pt, Rh and Pd catalysts supported on various $Ce_xZr_{1-x}O_2$ in the absence or presence of an electric field.

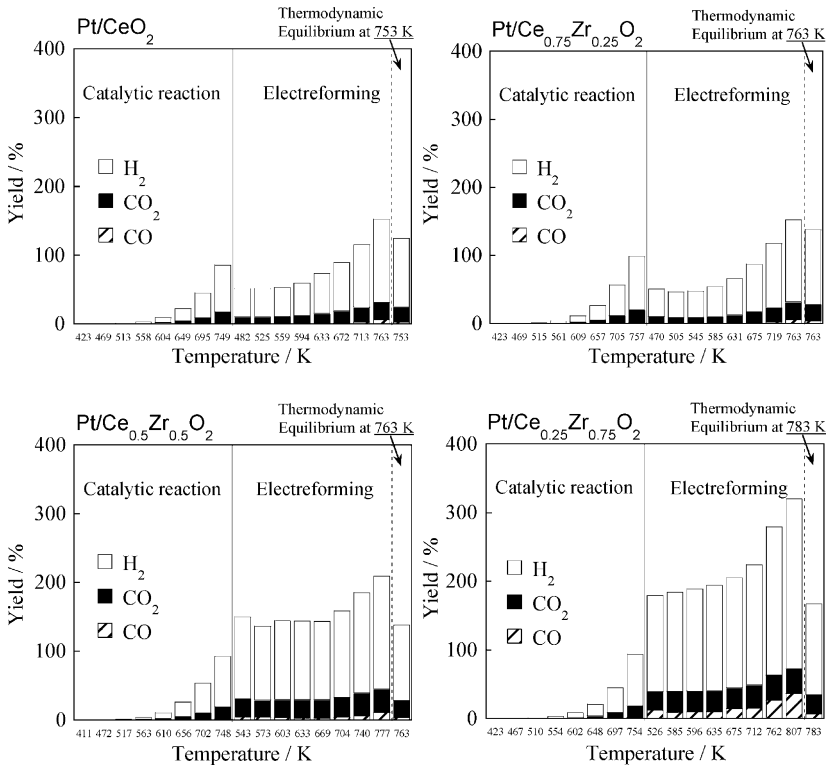

Fig. 6. Hydrogen, CO and CO_2 yield over Pt catalysts supported on various $Ce_xZr_{1-x}O_2$ with/without an electric field.

of Zr into CeO_2 on the electreforming. The methane conversion for electreforming increased with increasing zirconium content in the $Ce_xZr_{1-x}O_2$. In particular, $Pt/Ce_{0.25}Zr_{0.75}O_2$ exhibited the highest methane conversion, for example 39.1% at 526 K. For the other cases, methane conversion was 10.2% over $Pt/Ce_{0.75}Zr_{0.25}O_2$ at 470 K and 31.6% over $Pt/Ce_{0.5}Zr_{0.5}O_2$ at 543 K. The maximum conversion in the investigated range of the reaction temperature was 73.4% at 807 K over $Pt/Ce_{0.25}Zr_{0.75}O_2$. In the case of ZrO_2, we could not apply the electric field to the catalyst bed and we could not conduct electreforming due to its conductivity.

Fig. 6 shows the yield of products over each Pt-catalyst with/without application of electric field. From this figure it can be concluded that the products in the case of electreforming were about 80% H_2, 20% CO_2 and few percents of CO on the all Pt catalysts supported on $Ce_xZr_{1-x}O_2$, the trend being almost the same as that for the Pt/CeO_2 catalyst. For the catalytic reaction without electreforming over $Pt/Ce_xZr_{1-x}O_2$ catalyst, a similar trend was observed with that for Pt/CeO_2 catalyst. At low conversion level, the products over $Pt/Ce_xZr_{1-x}O_2$ catalyst were almost only H_2 and CO_2, while the ratio of CO to CO_2 increased for all catalysts with the increase in methane conversion due to the equilibrium limitation of water-gas shift reaction.

Table 3 indicates the formation rate of products and the endothermic enthalpy gain, ΔE_{ef} for Pt catalysts supported on $Ce_xZr_{1-x}O_2$. These energies at 423 K were 12.4–12.8 J min^{-1} for $Pt/Ce_{0.75}Zr_{0.25}O_2$, 30.1–32.4 J min^{-1} for $Pt/Ce_{0.5}Zr_{0.5}O_2$, 42.5–44.9 J min^{-1} for $Pt/Ce_{0.25}Zr_{0.75}O_2$. The input electric energies were 73.4–82.5 J min^{-1} (=1.22–1.37 W; $Pt/Ce_{0.75}Zr_{0.25}O_2$), 157.2–162.4 J min^{-1} (2.62–2.71 W; $Pt/Ce_{0.5}Zr_{0.5}O_2$), 169.8–211.4 J min^{-1} (=2.83–3.52 W; $Pt/Ce_{0.25}Zr_{0.75}O_2$). Therefore, about 16–26% of input electric energy was utilized to endothermic enthalpy gain by the electric field on the electreforming.

Other experiments under the same condition were conducted with Pd or Rh catalysts supported on $Ce_xZr_{1-x}O_2$. Results are included in Fig. 5. As presented in Fig. 5, the conversion increased greatly for all catalyst by the presence of electric field from the conversion for the reaction without electric field. In the case of using $Ce_{0.25}Zr_{0.75}O_2$ as support, the catalyst exhibited the highest conversion of methane, such as 42.3% at 544 K for $Rh/Ce_xZr_{1-x}O_2$. $Pd/Ce_xZr_{1-x}O_2$ and $Rh/Ce_xZr_{1-x}O_2$ resulted in a distribution of products similar to that for $Pt/Ce_xZr_{1-x}O_2$. These products were H_2, CO_2, CO.

Tables 4–6 shows ΔE_{ef} (endothermic enthalpy gain) at 423 K over Pd, Rh and Ni catalysts supported on. $Ce_xZr_{1-x}O_2$. From these tables, the amount of endothermic enthalpy gain for the electreforming over $Pd/Ce_xZr_{1-x}O_2$, $Rh/Ce_xZr_{1-x}O_2$ or $Ni/Ce_xZr_{1-x}O_2$ catalyst was 12–29% of the input electric energy.

Also we conducted experiments over catalysts without supported metal. Table 6 shows the experimental results for these cases, and we found that the catalyst support itself had little or no activity for the electreforming. So the active site of the steam reforming of methane by the electreforming requires supported metal and catalyst support which can conduct both oxygen ions and electrons (i.e. mixed conductor).

Fig. 7 shows the conversion for various metal catalysts supported on four $Ce_xZr_{1-x}O_2$ (X = 0, 0.25, 0.5, 0.75) supports. Here, X = 1, i.e. ZrO_2 was eliminated from the figure because ZrO_2 support was not applicable for electreforming. From these figures, the methane conversion for the electreforming increased as the ratio of Ce/Zr decreased. On the other hand, difference of activity among various metals seems small. This phenomenon indicated that the catalytic performance was enhanced by the interaction between electric field and the catalyst support with adding ZrO_2 to CeO_2.

3.3. Conversion/gas composition and thermodynamic equilibrium

To discuss the distribution of products for consecutive water gas shift reaction after steam reforming of methane, we investigated the interrelation between the methane conversion, CO/CO_2 composition and thermodynamic equilibrium temperature corresponding

Table 3
Activities and energy balances for Pt catalysts supported on $Ce_xZr_{1-x}O_2$ in the presence or absence of an electric field at 423 K of furnace temperature.

	EF[a]	T^b_{tc} (K)	CH_4 conv. (%)	ΔH_{CH4} (J min^{-1})	EPC[c] (W)	Formation rate (μmol min^{-1})			$H_2/(3CO+4CO_2)$	$\sum \Delta H^d_p$ (J min^{-1})	ΔH^e_r (J min^{-1})	ΔE_{ef} (J min^{-1})
						H_2	CO_2	CO				
$Pt/Ce_{0.75}Zr_{0.25}O_2$	No	423	0.0	0.0	–	0.0	0.0	0.0	–	0.0	0.0	
	With	470	10.2	45.6	1.37	203.6	50.3	1.0	1.0	58.5	12.8	12.8
$Pt/Ce_{0.5}Zr_{0.5}O_2$	No	411	0.0	0.0	–	0.0	0.0	0.0	–	0.0	0.0	
	With	543	31.6	131.9	2.71	554.3	127.1	21.0	1.0	164.4	32.4	32.4
$Pt/Ce_{0.25}Zr_{0.75}O_2$	No	423	0.0	0.0	–	0.0	0.0	0.0	–	0.0	0.0	
	With	526	39.1	180.2	2.83	725.2	139.6	62.8	1.0	225.0	44.9	44.9

[a] EF: electric field.
[b] T_{tc}: catalyst bed temperature measured by a thermocouple.
[c] EPC: electric power consumption for the electric field.
[d] $\sum \Delta H_p$ summation of the heating values of products.
[e] ΔH_r: difference of the heating rate of products and consumed methane.

Table 4
Activities and energy balances for Pd catalysts supported on $Ce_xZr_{1-x}O_2$ in the presence or absence of an electric field at 423 K of furnace temperature.

	EF[a]	T_{tc}[b] (K)	CH_4 conv. (%)	ΔH_{CH4} (J min^{-1})	EPC[c] (W)	Formation rate (μmol min^{-1})			$H_2/(3CO+4CO_2)$	$\sum \Delta H^d_p$ (J min^{-1})	ΔH^e_r (J min^{-1})	ΔE_{ef} (J min^{-1})
						H_2	CO_2	CO				
$Pd/Ce_{0.75}Zr_{0.25}O_2$	No	424	0.0	0.0	–	0.0	0.0	0.0	–	0.0	0.0	
	With	483	12.6	54.1	1.74	229.5	56.0	4.8	1.0	67.0	12.9	12.9
$Pd/Ce_{0.5}Zr_{0.5}O_2$	No	423	0.0	0.0	–	0.0	0.0	0.0	–	0.0	0.0	
	With	519	27.0	120.1	2.99	516.8	117.0	18.0	1.0	152.8	32.6	32.6
$Pd/Ce_{0.25}Zr_{0.75}O_2$	No	423	0.0	0.0	–	0.0	0.0	0.0	–	0.0	0.0	
	With	536	41.0	187.0	3.47	761.9	147.8	62.2	1.0	235.4	48.3	48.3

[a] EF: electric field.
[b] T_{tc}: catalyst bed temperature measured by a thermocouple.
[c] EPC: electric power consumption for the electric field.
[d] $\sum \Delta H_p$ summation of the heating values of products.
[e] $\sum \Delta H_r$: difference of the heating rate of products and consumed methane.

to these conversion/composition. Fig. 8 shows the methane conversion and the corresponding composition of CO/CO_2 in the products over $Pt/Ce_xZr_{1-x}O_2$. In addition, the equilibrium composition of CO/CO_2 was calculated and plotted in the figure. As presented in the figure, almost all the experimental points are along the equilibrium line. This shows that the water gas shift reaction after reforming methane reached equilibrium. Fig. 9 shows the relationship between the temperatures of catalyst bed measured by a thermocouple ($T_{thermocouple}$) and the temperature of equilibrium for water gas shift ($T_{WGS\ equilibrium}$) corresponding to the measured CO/CO_2 composition for $Pt/Ce_xZr_{1-x}O_2$ catalyst. As shown in the figure, $T_{WGS\ equilibrium}$ is higher than $T_{thermocouple}$. Thus in the methane electreforming, methane is activated by the catalyst surface due to the electric field, while the successive water gas shift reaction is regulated by the equilibrium at higher temperature than the exact temperature measured by a thermocouple.

3.4. The role of catalyst support

To investigate the role of catalyst support, we examined the specific surface area of the $Ce_xZr_{1-x}O_2$ support (Table 1). By adding ZrO_2 to CeO_2, the specific surface area increased, and $Ce_{0.25}Zr_{0.75}O_2$ had the highest surface area (55.0 m^2 g^{-1}) among all $Ce_xZr_{1-x}O_2$ and CeO_2 (7.2 m^2 g^{-1}). However, the conversion of methane for the electreforming using these $Ce_xZr_{1-x}O_2$ as a support did not follow a parallel trend. Although the specific surface area of $Ce_{0.5}Zr_{0.5}O_2$

Table 5
Activities and energy balances for Rh catalysts supported on $Ce_xZr_{1-x}O_2$ in the presence or absence of an electric field at 423 K of furnace temperature.

	EF[a]	T_{tc}[b] (K)	CH_4 conv. (%)	ΔH_{CH4} (J min^{-1})	EPC[c] (W)	Formation rate (μmol min^{-1})			$H_2/(3CO+4CO_2)$	$\sum \Delta H^d_p$ (J min^{-1})	ΔH^e_r (J min^{-1})	ΔE_{ef} (J min^{-1})
						H_2	CO_2	CO				
$Rh/Ce_{0.75}Zr_{0.25}O_2$	No	426	0.0	0.0	–	0.0	0.0	0.0	–	0.0	0.0	
	With	480	14.5	65.2	1.47	299.6	70.5	2.7	1.0	86.4	212	212
$Rh/Ce_{0.5}Zr_{0.5}O_2$	No	423	0.0	0.0	–	0.0	0.0	0.0	–	0.0	0.0	
	With	518	25.9	118.3	3.15	489.7	105.3	27.6	1.0	147.8	29.5	29.5
$Rh/Ce_{0.25}Zr_{0.75}O_2$	No	424	0.0	0.0	–	0.0	0.0	0.0	–	0.0	0.0	
	With	544	42.3	188.3	3.46	756.9	140.4	71.0	1.0	236.4	48.1	48.1

[a] EF: electric field.
[b] T_{tc}: catalyst bed temperature measured by a thermocouple.
[c] EPC: electric power consumption for the electric field.
[d] $\Sigma \Delta H_p$: summation of the heating values of products.
[e] ΔH_r: difference of the heating rate of products and consumed methane.

Table 6
Activities and energy balances for bare supports and Ni catalysts supported on $Ce_xZr_{1-x}O_2$ in the presence or absence of an electric field at 423 K of furnace temperature.

	EF[a]	T_{tc}[b] (K)	CH_4 conv. (%)	ΔH_{CH4} (J min^{-1})	EPC[c] (W)	Formation rate (μmol min^{-1})			H_2/(3CO + 4CO$_2$)	$\sum \Delta H^d_p$ (J min^{-1})	ΔH^e_r (J min^{-1})	ΔE_{ef} (J min^{-1})
						H_2	CO_2	CO				
$NiZCe_{0.75}Zr_{0.25}O_2$	No	425	0.0	0.0	–	0.0	0.0	0.0	–	0.0	0.0	
	With	463	12.1	54.7	1.29	241.2	56.2	5.3	1.0	70.4	15.7	15.7
$Ni/Ce_{0.5}Zr_{0.5}O_2$	No	425	0.0	0.0	–	0.0	0.0	0.0	–	0.0	0.0	
	With	482	19.1	85.1	1.53	354.9	81.2	14.3	1.0	105.5	20.4	20.4
$NiZCe_{0.25}Zr_{0.75}O_2$	No	427	0.0	0.0	–	0.0	0.0	0.0	–	0.0	0.0	
	With	535	41.6	191.5	3.54	708.8	126.2	84.6	0.9	229.7	38.1	38.1
$Ni/SrTiO_3$	No	425	0.0	0.0	–	0.0	0.0	0.0	–	0.0	0.0	
	With	499	2.9	11.7	2.67	49.0	12.2	0.6	1.0	14.5	2.8	2.8
CeO_2	No	416	0.0	0.0	–	0.0	0.0	0.0	–	0.0	0.0	
	With	479	1.3	6.1	1.31	15.1	1.2	2.1	1.3	7.5	1.4	1.4
$SrTiO_3$	No	422	0.0	0.0	–	0.0	0.0	0.0	–	0.0	0.0	
	With	492	0.5	2.2	2.45	7.6	0.4	1.4	1.3	3.1	0.9	0.9

[a] EF: electric field.
[b] T_{tc}: catalyst bed temperature measured by a thermocouple.
[c] EPC: electric power consumption for the electric field.
[d] $\sum \Delta H_p$: summation of the heating values of products.
[e] ΔH_r: difference of the heating rate of products and consumed methane.

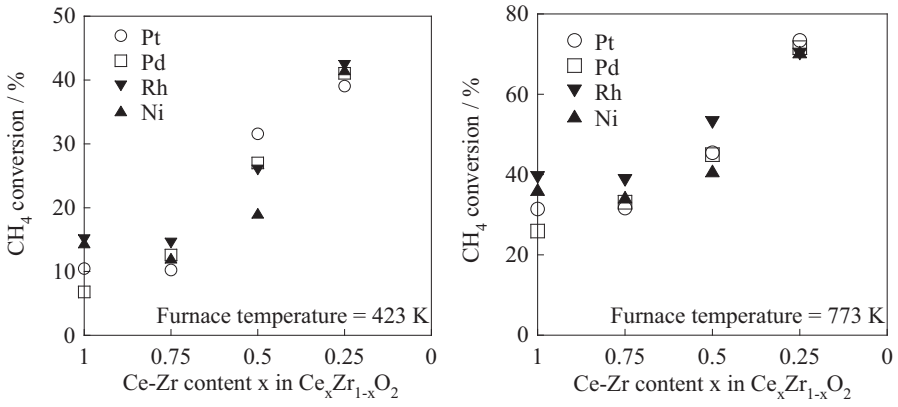

Fig. 7. Effect of Ce/Zr ratio on the methane conversion under electreforming.

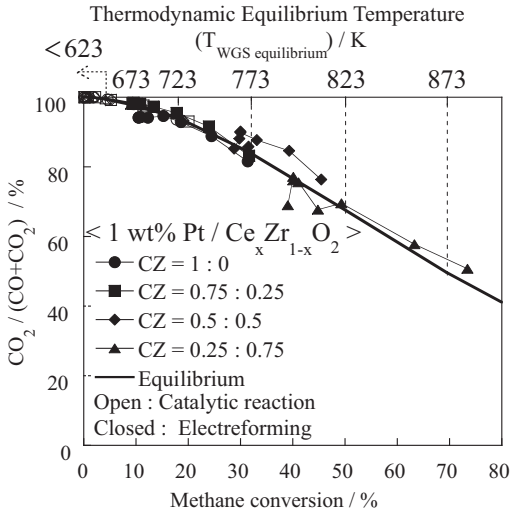

Fig. 8. Methane conversion, selectivity to CO/CO_2 and thermodynamic equilibrium temperature over Pt catalysts supported on various $Ce_xZr_{1-x}O_2$ under electreforming conditions.

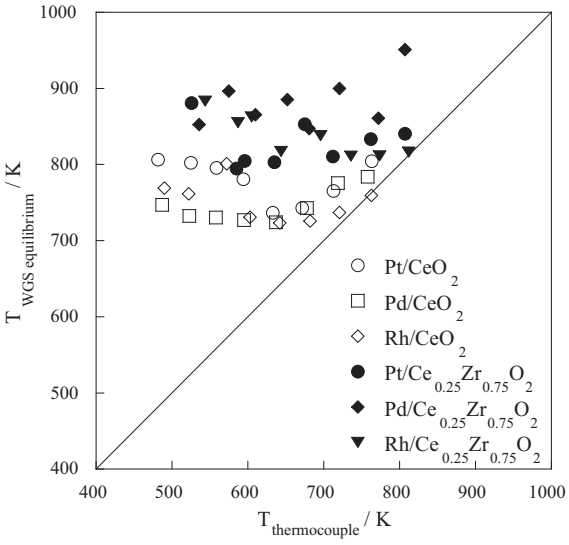

Fig. 9. Relation between catalyst bed temperature ($T_{thermocouple}$) and temperature calculated from thermodynamic equilibrium for the same conversion over various catalysts under electreforming conditions.

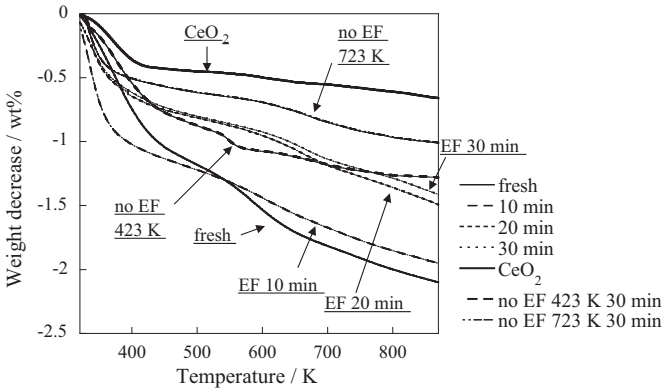

Fig. 10. TPR profiles of Pt/CeO_2 catalysts before/after electreforming or conventional catalytic reaction.

number	D / nm	
	fresh	used 30min
①	33.4	35.2
②	29.5	32.9
③	27.5	32.1
④	28.5	33.4

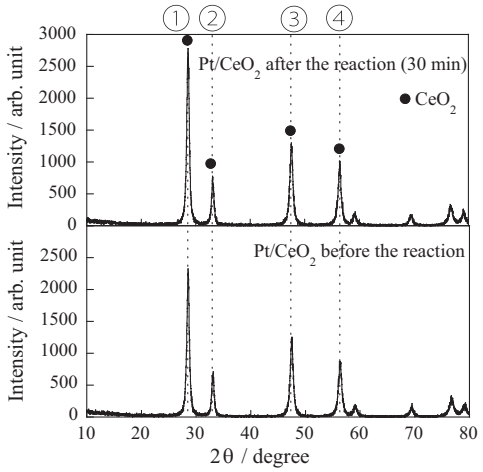

Fig. 11. XRD patterns of Pt/CeO_2 catalysts before/after electreforming.

($53.2\,m^2\,g^{-1}$) and $Ce_{0.25}Zr_{0.75}O_2$ ($55.0\,m^2\,g^{-1}$) were similar, the conversion of methane for electreforming showed a large difference between $Pt/Ce_{0.5}Zr_{0.5}O_2$ and $Pt/Ce_{0.25}Zr_{0.75}O_2$. Therefore, the observed difference of the catalytic activity for electreforming by changing zirconium content in $Ce_xZr_{1-x}O_2$ was independent of the surface area of $Ce_xZr_{1-x}O_2$.

Here, we would like to consider the role of CeO_2 or $Ce_xZr_{1-x}O_2$ as a catalyst support on the electreforming. CeO_2 has been applied widely as catalysts for steam reforming of methane or water gas shift (WGS) reaction and other oxidation reactions [50–56]. CeO_2 as catalyst or support shows high activity and/or high selectivity, derived from its redox property and high oxygen storage capacity (OSC) [54–56]. On the other hand, addition of ZrO_2 to CeO_2 ($Ce_xZr_{1-x}O_2$) is known to enhance the activity of CeO_2 for oxidation reactions compared to pure CeO_2 [57–61]. The high availability of surface oxygen for the oxidation of surface adsorbants explains the high activity of $Ce_xZr_{1-x}O_2$. By introducing Zr into CeO_2, other effects such as improvement of surface area [60,61], increased stability of the catalytic activity [62], high dispersion of supported metal [63] have also been reported. Furthermore, the high oxidative function of $Ce_xZr_{1-x}O_2$ has been assumed to be a good redox property [64–68]. This has been attributed to an increased oxygen mobility and an increased activity for the Ce^{4+}/Ce^{3+} redox resulting from the creation of surface and bulk defects in the $Ce_xZr_{1-x}O_2$, induced by the introduction of the smaller Zr^{4+} cation in the fluorite lattice. K. Otsuka et al. [65] reported that the gas–solid reaction between methane and oxidatively treated CeO_2–ZrO_2 at 1073 K produced in the absence of gaseous oxidant at 973 K synthesis gas with a H_2/CO ratio of 2. This result suggested that methane, as reductant, reduced cerium in the CeO_2–ZrO_2 from Ce^{4+} to Ce^{3+}. The reaction was further accelerated by the presence of Pt, and the degree of reduction was nearly tripled compared to that in the absence of Pt at 773 K. Although bare CeO_2 is reduced around 773 K in reducing atmosphere, $Ce_xZr_{1-x}O_2$ is reduced at lower temperature as 655 K [66,67]. Furthermore, the chemical composition, that is Zr contents in CeO_2–ZrO_2, had an influence on the reducibility of Ce^{4+} sites. The reduction of the diamagnetic Ce^{4+} ions of the CeO_2–ZrO_2 into paramagnetic Ce^{3+} species due to formation of oxygen vacancies was exhibited by magnetic susceptibility measurements using a Faraday microbalance. In this paper, we observed increase of activity for electreforming by doping Zr into CeO_2 while we have already found that the reducibility of lattice oxygen on the catalyst support plays an important role for the electreforming.

To investigate the consumption of lattice oxygen of $Ce_xZr_{1-x}O_2$ after the electreforming reaction, we conducted TPR (temperature programmed reduction) of the catalyst before/after the reaction. The results are shown in Fig. 10 and reveal that the surface lattice oxygen is consumed under electreforming. This observation supports the importance of redox ability of the catalyst support. Furthermore, the confirmed effect of Zr-doping into CeO_2 is in agreement with the TPR results. After reaction, the crystalline structure of the catalyst support was also confirmed by XRD (Fig. 11). As shown in Fig. 11, there is no peak-shift derived from the distortion of bulk structure. From these results of TPR and XRD, it is concluded that the electreforming consumed only the surface lattice oxygen on $Ce_xZr_{1-x}O_2$, and that the consumed lattice oxygen on $Ce_xZr_{1-x}O_2$ was regenerated by steam in the reaction mixture atmosphere. If the regeneration ceased, catalytic activity would decrease with the time course of electreforming. However we have not observed any deactivation of the activity of the catalyst for electreforming.

To investigate the reason for the promotion of catalytic activity by electreforming, we tried other on–off tests using several catalysts [48]. By applying an electric field on the catalyst bed, hydrogen and carbon dioxide were produced immediately. After turning off the electric field the production ceased. Thermodynamic equilibrium analysis and temperature measurements using IR and a thermocouple showed that promotion of the catalytic activity by the electric field was not due to the heat supplied by the electric field. We observed this enhancement of the activity of catalyst by impressing the electric field in other cases (reactants, catalysts) [49]. From observation of the waveforms of current and voltage using an oscilloscope, this electric field is apparently a kind of dark current/dark discharge. We observed no light emission from the catalyst bed, so it was not a kind of plasma.

Our experimental results in this paper revealed that the redox ability of support was very important for the electreforming, and the supported metal was also required for the activity. So we concluded that the high activity of the electreforming at low temperature was derived from the synergetic effect between the high redox ability of catalyst support and the dark current/dark discharge on the catalyst onto the supported metal.

4. Conclusion

In this paper we conducted catalytic steam reforming of methane at low temperature in an electric field. Results show that catalytic steam reforming of methane was drastically promoted

in an electric field. We found that metal catalysts supported on $Ce_xZr_{1-x}O_2$ showed higher activity. Gas phase temperature measured by a thermocouple was very low, while the conversions of methane steam reforming and water gas shift showed that the equilibrium of the electreforming was determined by a high electron temperature. We confirmed that the surface lattice oxygen played an important role for the electreforming, and the catalyst surface would be reduced by methane and oxidized by steam (redox mechanism).

References

[1] J.R. Rostrup-Nielsen, Phys. Chem. Chem. Phys. 3 (2001) 283.
[2] J.R. Rostrup-Nielsen, Catal. Today 111 (2006) 4.
[3] J. Wei, E. Iglesia, J. Catal. 224 (2004) 370.
[4] D. Trimm, Catal. Today 49 (1999) 3.
[5] J.D. DeRen, P.G. Menon, G.F. Froment, G. Haemers, J. Catal. 70 (1981) 225.
[6] V.R. Choudhary, A.M. Rajput, Ind. Eng. Chem. Res. 35 (1996) 3934.
[7] K. Urasaki, Y. Sekine, S. Kawabe, E. Kikuchi, M. Matsukata, Appl. Catal. A: Gen. 286 (2005) 23.
[8] T. Hayakawa, S. Suzuki, J. Nakamura, T. Uchijima, S. Hamakawa, K. Suzuki, T. Shishido, K. Takehira, Appl. Catal. A: Gen. 183 (1999) 273.
[9] A.I. Tsyganok, T. Tsunoda, S. Hamakawa, K. Suzuki, K. Takehira, T. Hayakawa, J. Catal. 213 (2003) 191.
[10] T. Numaguchi, Catal. Surv. Jpn. 5 (2001) 59.
[11] O. Yamazaki, K. Tomishige, K. Fujimoto, Appl. Catal. A: Gen. 136 (1996) 49.
[12] B. Li, R. Watanabe, K. Maruyama, K. Kunimori, K. Tomishige, Catal. Today 104 (2005) 7.
[13] B. Li, S. Kado, Y. Mukainakano, M. Nurunnabi, T. Miyao, S. Naito, K. Kunimori, K. Tomishige, Appl. Catal. A: Gen. 304 (2006) 62.
[14] Y. Mukainakano, B. Li, S. Kado, T. Miyazawa, K. Okumura, T. Miyao, S. Naito, K. Kunimori, K. Tomishige, Appl. Catal. A: Gen. 318 (2007) 252.
[15] D.G. Löffler, K. Taylor, D. Mason, J. Power Sources 117 (2003) 84.
[16] J. Armor, Appl. Catal. A: Gen. 176 (1999) 159.
[17] S.C. Reyes, J.H. Sinfelt, J.S. Feeley, Ind. Eng. Chem. Res. 42 (2003) 1588.
[18] D.A. Hickman, L.D. Schmidt, J. Catal. 138 (1992) 267.
[19] D.A. Hickman, L.D. Schmidt, Science 259 (1993) 343.
[20] R. Horn, K.A. Williams, N.J. Degenstein, L.D. Schmidt, Chem. Eng. Sci. 62 (2007) 1298.
[21] T. Kirchner, G. Eigenberger, Chem. Eng. Sci. 51 (1996) 2409.
[22] K. Kollmann, J. Abthoff, W. Zahn, SAE Tech. Pap. (1994) 940469.
[23] H. Jung, W.L. Yoon, H. Lee, J.S. Park, J.S. Shin, H. La, J.D. Lee, J. Power Source 124 (2003) 76.
[24] Y. Iwasaki, J. Liu, J. Zhang, T. Kitajima, M. Sakurai, H. Kameyama, J. Chem. Eng. Jpn. 39 (2006) 216.
[25] Y. Xing, Z. Liu, R.A. Couttenye, W.S. Willis, S.L. Suib, P.T. Fanson, H. Hirata, M. Ibe, J. Catal. 250 (2007) 67.
[26] S.L. Suib, R.P. Zerger, J. Catal. 139 (1993) 383.
[27] C.J. Liu, A. Marafee, B. Hill, G. Xu, R. Mallinson, L. Lobban, Ind. Eng. Chem. Res. 35 (1996) 3295.
[28] O. Mutaf-yardimci, A.V. Saveliev, A.A. Fridman, L.A. Kennedy, Int. J. Hydrogen Energy 12 (1998) 1109.
[29] S. Kado, Y. Sekine, K. Fujimoto, Chem. Commun. (1999) 2485.
[30] Y. Sekine, J. Yamadera, M. Matsukata, E. Kikuchi, Chem. Eng. Sci. 65 (2010) 487.
[31] Y. Sekine, S. Asai, S. Kado, M. Matsukata, E. Kikuchi, Chem. Eng. Sci. 63 (2008) 5056.
[32] Y. Sekine, K. Urasaki, S. Kado, M. Matsukata, E. Kikuchi, Energy Fuels 18 (2004) 455.
[33] S. Kado, K. Urasaki, Y. Sekine, K. Fujimoto, Chem. Commun. (2001) 415.
[34] Y. Inoue, Y. Watanabe, T. Noguchi, J. Phys. Chem. 99 (1995) 9898.
[35] M. Stoukides, C.G. Vayenas, J. Catal. 64 (1980) 18.
[36] C.G. Vayenas, S. Bebelis, S. Ladas, Nature 343 (1990) 625.
[37] C.G. Vayenas, S. Bebelis, S. Neophytides, J. Phys. Chem. 92 (1988) 5083.
[38] S. Bebelis, C.G. Vayenas, J. Catal. 118 (1989) 125.
[39] M. Ouzounidou, A. Skodra, C. Kokkofitis, M. Stoukides, Solid State Ionics 178 (2007) 153.
[40] S. Bebelis, N. Kotsionopoulos, Solid State Ionics 177 (2006) 2205.
[41] V.D. Belyaev, T.I. Politova, V.A. Sobyanin, Solid State Ionics 136–137 (2000) 721.
[42] V.A. Sobyanin, V.D. Belyaev, React. Kinet. Catal. Lett. 51 (1993) 373.
[43] N.A. Anastasijevic, Catal. Today 146 (2009) 308.
[44] A. de Lucas-Consuegra, F. Dorado, J.L. Valverde, R. Karoum, P. Vernoux, J. Catal. 251 (2007) 474.
[45] C. Jimenez-Borja, F. Dorado, A. de Lucas-Consuegra, J.M. Garcia-Vargas, J.L. Valverde, Catal. Today 146 (2009) 326.
[46] I. Riess, Solid State Ionics 176 (2005) 1667.
[47] B. Delmon, Catal. Today 117 (2006) 69.
[48] Y. Sekine, M. Tomioka, M. Matsukata, E. Kikuchi, Catal. Today 146 (2009) 183.
[49] Y. Sekine, M. Haraguchi, M. Tomioka, M. Matsukata, E. Kikuchi, J. Phys. Chem. A 114 (2010) 3824.
[50] S. Xu, X. Yan, X. Wang, Fuel 85 (2006) 2243.
[51] W. Cai, B. Zhang, Y. Li, Y. Xu, W. Shen, Catal. Commun. 8 (2007) 1588.
[52] E.S. Ranganathan, S.K. Bej, L.T. Thompson, Appl. Catal. A: Gen. 289 (2005) 153.
[53] D. Andreeva, V. Idakiev, T. Tabakova, L. Ilieva, P. Falaras, A. Bourlinos, A. Travlos, Catal. Today 72 (2002) 51.
[54] F. Frusteri, S. Freni, V. Chiodo, S. Donato, G. Bonura, S. Cavallaro, Int. J. Hydrogen Energy 31 (2006) 2193.
[55] N. Laosiripojana, S. Assabumrungrat, Appl. Catal. B: Environ. 66 (2006) 29.
[56] P. Pantu, G.R. Gavalas, Appl. Catal. A: Gen. 223 (2002) 253.
[57] P. Biswas, D. Kunzru, Int. J. Hydrogen Energy 32 (2007) 969.
[58] P. Biswas, D. Kunzru, Chem. Eng. J. 136 (2008) 41.
[59] H. Roh, Y. Wang, D.L. King, A. Platon, Y. Chin, Catal. Lett. 108 (2006) 15.
[60] S. Xu, X. Wang, Fuel 84 (2005) 563.
[61] C. Diagne, H. Idriss, A. Kiennemann, Catal. Commun. 3 (2002) 565.
[62] H. Oguchi, T. Nishiguchi, T. Matsumoto, H. Kanai, K. Utani, Y. Matsumura, S. Imamura, Appl. Catal. A: Gen. 281 (2005) 69.
[63] V. Perrichon, L. Retailleau, P. Bazin, M. Daturi, J.C. Lavalley, Appl. Catal. A: Gen. 260 (2004) 1.
[64] C. Leitenburg, A. Trovarelli, J. Llorca, F. Cavani, G. Bini, Appl. Catal. A: Gen. 139 (1996) 161.
[65] K. Otsuka, Y. Wang1, M. Nakamura, Appl. Catal. A: Gen. 183 (1999) 317.
[66] H. Vidal, J. Kašpar, M. Pijolat, G. Colonb, S. Bernal, A. Cordón, V. Perrichon, F. Fally, Appl. Catal. B: Environ. 27 (2000) 49.
[67] F. Fally, V. Perrichon, H. Vidal, J. Kaspar, G. Blanco, J.M. Pintado, S. Bernal, G. Colon, M. Daturi, J.C. Lavalley, Catal. Today 59 (2000) 373.
[68] E.M. Sadovskaya, Y.A. Ivanova, L.G. Pinaeva, G. Grasso, T.G. Kuznetsova, A. Veen, V.A. Sadykov, C. Mirodatos, J. Phys. Chem. A 111 (2007) 4498.